ISSN 1392–1207. MECHANIKA. 2014 Volume 20(6): 590–595

Experimental analysis and numerical simulation of the stainless AISI 304 steel friction drilling process

P. Krasauskas*, S. Kilikevičius, R. Česnavičius***, D. Pačenga******

**Kaunas University of Technology, Studentų 56, 51424, Kaunas, Lithuania, E-mail: povilas.krasauskas@ktu.lt*
***Kaunas University of Technology, Studentų 56, 51424, Kaunas, Lithuania, E-mail: sigitas.kilikevicius@ktu.lt*
****Kaunas University of Technology, Studentų 56, 51424, Kaunas, Lithuania, E-mail: ramunas.cesnavicius@ktu.lt*
*****Kaunas University of Technology, Studentų 56, 51424, Kaunas, Lithuania, E-mail: domas.pacenga@stud.ktu.lt*

crossref http://dx.doi.org/10.5755/j01.mech.20.6.8664

1. Introduction

Thread machining is a widely used manufacturing process. However, sometimes its applicability is complicated due to the insufficient thickness of a workpiece, for example, during thread tapping in thin-walled parts.

Therefore, various design decisions in the automotive industry, furniture manufacturing and other applications, such as speed nuts and clips, for joining irresponsible parts, fasteners, square weld nuts, riveted anchors for a reliable fixture of parts are used. Usage of these fastening methods requires additional elements and technological operations, so it makes the manufacturing process more labour expenditure.

For this reason, non-traditional drilling and tread tapping processes are used. One of them is friction drilling, which is carried out using a special tungsten carbide tool. Applying this method, the metal becomes plastic due to significantly increased temperature in the drilling zone caused by the friction between the tool and the workpiece and, as a consequence, the tool penetrates the workpiece material. At that time, the tool forms an additional molten flange (a neck) on the underneath side of the sheet, which later can be frictionally tapped using a special tapper.

The main stages of the friction drilling process are presented in Fig. 1.

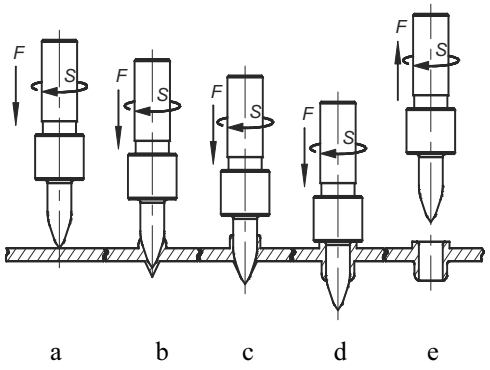

Fig. 1 Friction drilling stages: a – initial contact; b – tool-tip penetration into the material; c – material flow and hole forming; d – bush forming; e – tool withdrawal

When a rotating punch-type tool is forced into a metal strip, the heat, generated from the friction between the tool and plate surfaces, heats the surrounding zone up to 700 – 900 C. Therefore, the material becomes plastic and the tool forms a cylindrical hole without removal of the metal. The excess of the material forms a neck on the lower side of the hole and a bushing on the upper side of the sheet, by these means increasing the wall thickness and strength of the hole.

The literature review on the subject showed that experimental investigations and numerical simulations of the influence of mechanical and physical properties on the friction drilling process was mainly carried out on aluminium, magnesium and stainless steel alloys [1-3]. The majority of works dealing with frictional drilling of stainless steel [4, 5] are focused only on experimental investigations and analyse the drilling force and moment along with surface roughness of the drilled holes and tool wear. The review showed that the numerical simulation of this process is conditioned by a lot of conventionalities and uncertainties as well as highly depend on various factors such as material properties, drilling regimes, geometrical parameters of a tool and a workpiece, etc. [1, 2], therefore a numerical simulation of friction drilling for each new material is complicated and specific. Besides, the influence of cutting regimes was investigated in very short range. Since this method is a recently new metal machining method, the friction drilling process still is not investigated deep enough.

The purpose of our investigation was to perform drilling experiments of AISI 304 steel, to obtain drilling parameters, to perform a simulation of the process and to compare results with the experimental ones.

2. Materials and experiment technique

Drilling experiment was performed using AISI 304 steel sheet strips with 1.5 mm in thickness.

The chemical composition of the steel as received is presented in Table 1.

Table 1

Chemical composition of AISI 304 steel

C, %	Mn, %	P, %	S, %	Cr, %	Ni, %	Si, %
0.08	2.0	0.0045	0.03	18-20	8–10.5	1.0

The experiments were carried out on a CNC milling machine “DMU-35M” with a “Sinumerik 810D/840D” controller and “ShopMill” software using a tungsten carbide tool with a diameter of 5.2 mm. The experimental setup is shown in Fig. 2.

The axial force and torque were measured using a universal laboratory charge amplifier Kistler type 5018A and a press force sensor Kistler type 9345B mounted on the CNC table. Measuring ranges of the sensor: -10…10 kN for force, -25...25 Nm for torque; sensitivity: ≈-3.7 pC/N for force, ≈-200 pC/Nm for torque. The amplifier converts the charge signal from the piezoelectric pressure sensor into a proportional output voltage.

The variation of the axial drilling force and torque was recorded to a computer using a "PICO ADC-212" oscilloscope. The drilling temperature on the upper side of the plate at the contact zone was measured using a "Fluke574" optical pyrometer (measuring range: -30…900°C; accuracy: ±0.75% of reading; response time 250 ms) and recorded to the computer as well.

Fig. 2 Experimental setup of the friction drilling experiment

3. Experimental results and discussion

During the experiment, spindle rotation speed was set to 3000 rpm and the drilling feed rate of 100 mm/min was assigned.

The experimental axial force and torque variation is shown in Fig. 3.

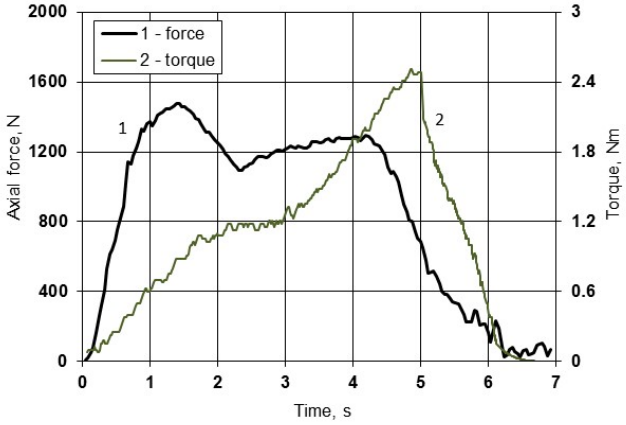

Fig. 3 Experimental axial force *1* and torque *2* variation during hole forming

An analysis of the experimental data showed that the axial force, during the drilling process (from the initial contact until the end of the hole forming) varies in a very wide range. It was defined, that the axial force reaches its maximum value when the conical part of the tool fully penetrates into the strip ("b" step, Fig. 1). When the sheet is pierced, the axial force drastically decreases ("c" step), meanwhile the torsion moment increases. The maximum torque is reached in the "c" step of hole forming when the conical part of the tool is fully penetrated into the sheet. The force is increasing again when the tool on the upper sheet surface forms a bushing ("d" step).

The experiment showed that the maximum axial drilling force for a 1.5 thickness sheet of AISI 304 steel is about 1480 N and the maximum torque is up to 2.5 Nm. The measured temperature on the upper side of the plate at the contact zone reaches 569°C.

4. Theoretical background of the friction drilling process

During friction drilling, heat is generated from two sources: plastic energy dissipation due to the shear deformation and heating due to the friction in the tool and workpiece contact zone.

The heating from the friction between the tool and the workpiece is the main heat source and comprises 98-99% of the total heat, therefore the heat transfer during tool penetration into workpiece is described [2]:

$$\rho c \frac{\partial T}{\partial t} = \left[k_x \frac{\partial^2 T}{\partial x^2} + k_y \frac{\partial^2 T}{\partial y^2} + k_z \frac{\partial^2 T}{\partial z^2} \right] + \dot{q}_f , \qquad (1)$$

where ρ is the material density; c is the specific heat, T is the temperature, t is the time, k is the heat conductivity in x, y, and z coordinates; $\dot{q}_f$ is the heat generated by the friction between the tool and the workpiece, it is expressed:

$$\dot{q}_f = \int_0^{T_f} \omega \, dT_f , \qquad (2)$$

where ω is the angular velocity of the tool and T_f is the friction moment in the contact zone.

For the finite element method simulation the temperature and strain rate dependent Johnson-Cook model was used [6]. In this case, the flow stress is expressed:

$$\bar{\sigma} = \left(A + B \left(\bar{\varepsilon}_{pl} \right)^n \right) \left[1 + C \ln \frac{\dot{\bar{\varepsilon}}_{pl}}{\dot{\varepsilon}_0} \right] \left(1 - \left(\frac{\theta - \theta_{tran}}{\theta_{melt} - \theta_{tran}} \right)^m \right), \qquad (3)$$

where parameter A is the initial yield strength of the material at room temperature, B is the hardening modulus; C is the parameter representing strain rate sensitivity; $\bar{\varepsilon}_{pl}$ is the effective plastic strain; $\dot{\bar{\varepsilon}}_{pl}$ is the effective plastic strain rate $\dot{\varepsilon}_0$ is the reference strain rate; n is the strain hardening exponent; m is the parameter which evaluates thermal softening effect, θ is temperature, θ_{melt} and θ_{tran} are material the melting and transition temperatures.

A failure criterion is required to characterize the material properties degradation due to the tool penetration into the material. The Johnson–Cook failure model based on the plastic strain was used in this study. In this model, failure occurs when the parameter D reaches a value of 1:

$$D = \int \frac{1}{\varepsilon_f} d\bar{\varepsilon}_{pl} . \qquad (4)$$

The equivalent strain to fracture ε_f is defined by [7]:

$$\varepsilon_f = \left(d_1 + d_2 e^{-d_3 \frac{p}{\sigma}} \right) \left[1 + d_4 \ln \frac{\dot{\bar{\varepsilon}}_{pl}}{\dot{\varepsilon}_0} \right] \left(1 + d_5 \theta \right), \qquad (5)$$

where d_1 to d_5 are material constants, which can be determined from experiments, p is the hydrostatic pressure, i.e. the third of the trace of the Cauchy stress tensor.

5. Finite element model of the friction drilling process

A three-dimensional geometry model of the tool and the workpiece was created in SolidWorks software and imported in ABAQUS/EXPLICIT finite element analysis software. The workpiece was created as a disk of 18 mm diameter and 1.5 mm thickness. The 3D model and dimensions of the tool are presented in Fig. 4.

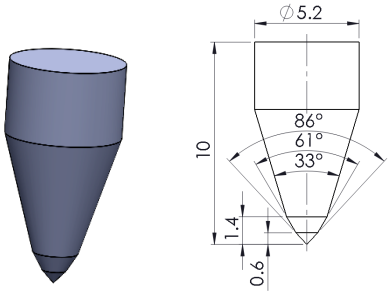

Fig. 4 3D model and dimensions of the tool

One of the primary difficulties in the simulation is the excessive mesh distortion in the plunge phase, so ABAQUS/EXPLICIT finite element code based on the adaptive mesh technique, allows automatically regenerate the mesh when the elements due to large deformation are distorted. The adaptive meshing technique in ABAQUS/EXPLICIT creates a new mesh and remaps the solution parameters from the existing mesh to the newly created mesh. In this study, the adaptive meshing was carried out for every three increments of the tool and five mesh sweeps per adaptive mesh increment was performed. The tool and the workpiece was meshed using element type C3D8RT, which has 8-node tri-linear displacement, temperature and reduced integration with hourglass control. A global element size of 0.3 mm was used to mesh the workpiece. An element size of 0.15 mm was used in the center of the workpiece where the tool penetrates the material. 10 layers of elements through the thickness were generated in the workpiece. The mesh of the workpiece contained 89710 elements. The mesh is shown in Fig. 5.

In order to save computational time, the mass scaling technique that modifies the densities of the materials in the model and improves the computational efficiency was used [8]. In this study, mass scaling was performed every 10 increments to obtain a stable time increment of at least 0.0001 s step time.

It was assumed that the tool is rigid and adiabatic, the frictional contact is described by Coulomb's friction law with the constant coefficient of friction μ and 100% of dissipated energy caused by friction between the parts was converted to heat. The coefficient of friction was set to 0.1.

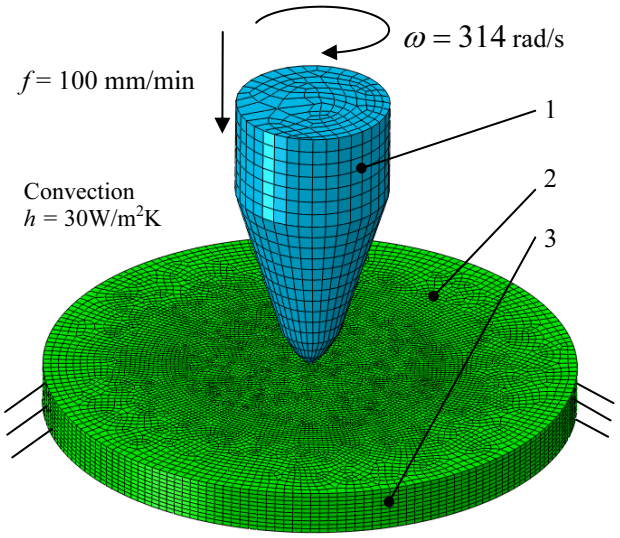

Fig. 5 Mesh and boundary conditions: *1* – the drilling tool; *2* – the workpiece; *3* – the fixed surface of the workpiece

The boundary conditions (Fig. 5) were set as follow: the outer surface of the workpiece was fixed in all degree of freedom; the top and bottom surfaces of the workpiece were under free convection with the convection coefficient of 30 W/m^{2}K; the ambient air temperature and the initial temperature of the workpiece were set to 295 K (22ºC). The tool rotation was set to 3000 rpm and the feed rate to 100 mm/min.

Material properties and the Johnson-Cook parameters used for the simulation of the drilling process are presented in Table 2 [9].

Table 2

AISI 304 steel properties and the Johnson-Cook parameters

Parameter	Units	Value
Young modulus, E	MPa	207.8
Poisson's ratio, v	-	0.3
Density, ρ	N/m^3	8000
Melting temperature, θ_{melt}	K	1673
Transition temp, θ_{tran}	K	1000
Specific heat capacity	J/(kgK)	452
Thermal expansion, α_L	10^{-6} K^{-1}	17.8
Initial yield strength A	MPa	280
Hardening modulus B	MPa	802.5
Strain hardening exponent n	-	0.622
Thermal softening exponent m	-	1.0
Strain rate constant C	-	0.0799
Reference strain rate $\dot{\varepsilon}_0$	1/s	1.0

The Jonson-Cook material damage parameters used in the simulation were as follow: $d_1 = 0.69$, $d_2 = d_3 = d_5 = 0$, $d_4 = 0.0546$ [9].

6. Numerical simulation and comparison to the experimental results

The simulation of the friction drilling process was carried out ant results were obtained.

Figs. 6 and 7 show how the equivalent plastic strain and the Von Mises stress change during the drilling process. Throughout the whole process, the maximum value of equivalent plastic strain was 2.39.

The simulation showed that the maximum temperature is reached when the conical part of the tool penetrates the workpiece. It is up to 1180 K (907°C) (Fig. 8, c) at that moment. The temperature is up to 969 K (696°C) in the final stage of the drilling (Fig. 8, d).

Figs. 6 and 7 show that the shape of workpiece deformation i.e. formation of the neck is close to the actual shape obtained by the experiments.

Dependencies of the axial force (Fig. 9, a) and the torque (Fig. 9, b) on time were obtained and compared to the experimental ones. The profiles of the experimental and simulated dependencies were quite similar.

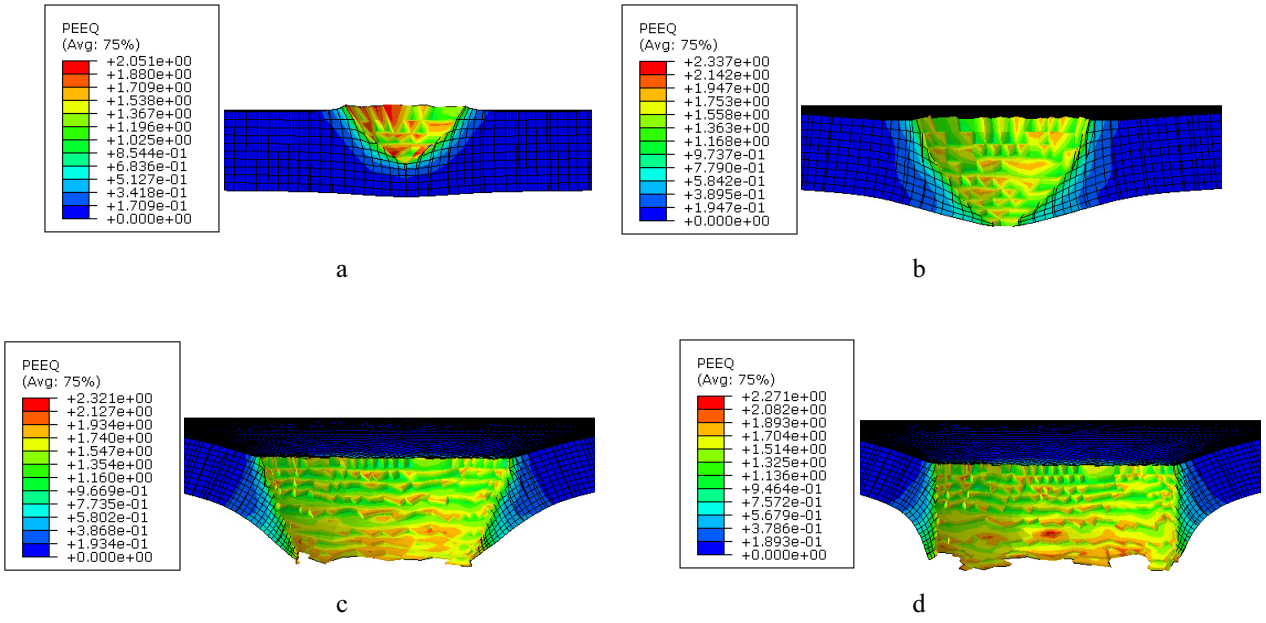

Fig. 6 Equivalent plastic strain in the workpiece at various distances of tool travel: a – 1 mm; b – 2.5 mm; c – 8 mm d – 12 mm

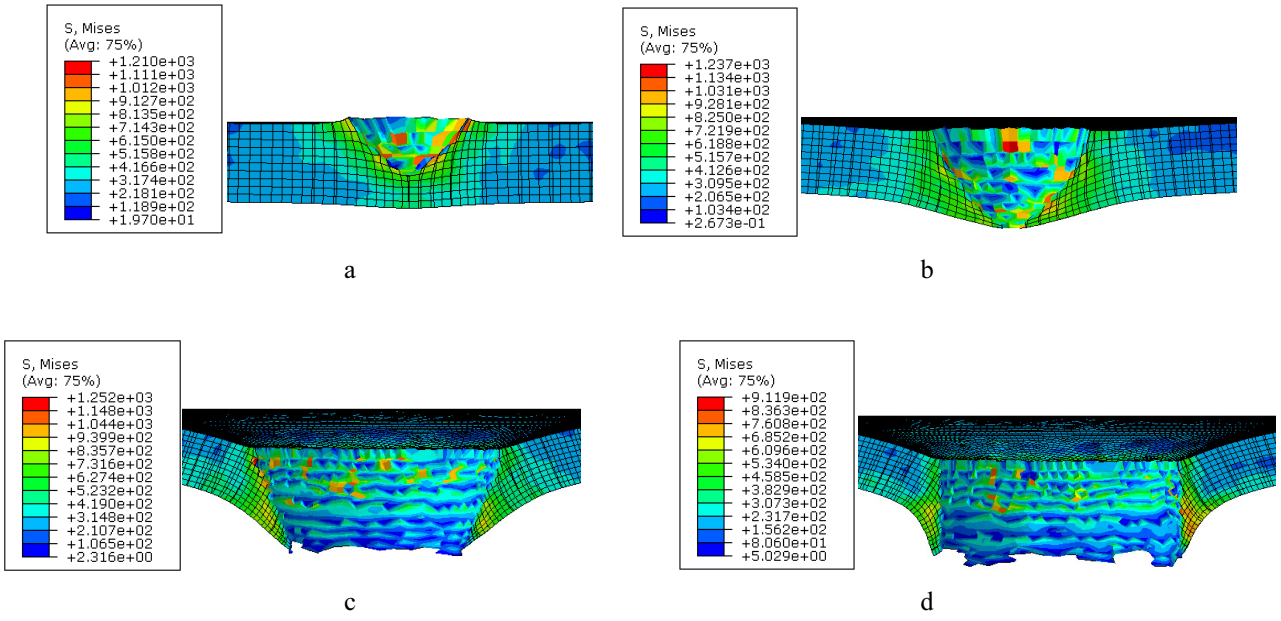

Fig. 7 Von Mises stress (units are in MPa) in the workpiece at various distances of tool travel: a – 1 mm; b – 2.5 mm; c – 8 mm ; d – 12 mm

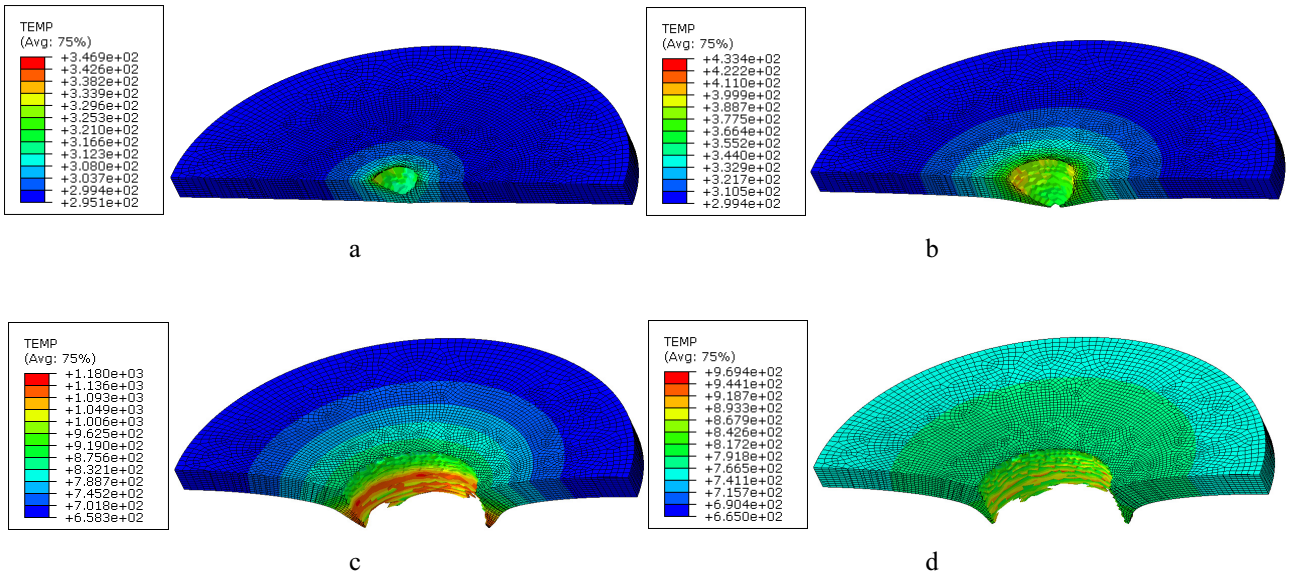

Fig. 8 Workpiece temperature (units are in K) at various distances of tool travel: a – 1 mm; b – 2.5 mm; c – 9.7 mm d – 12 mm

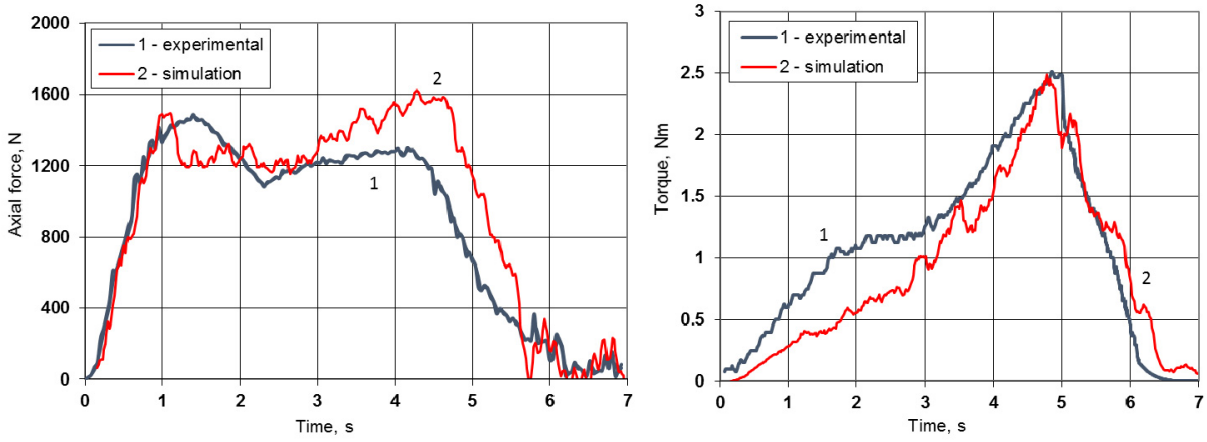

Fig. 9 Axial force (a) and torque (b) variation

A temperature variation on the upper side of the workpiece at the contact zone is shown in Fig. 10.

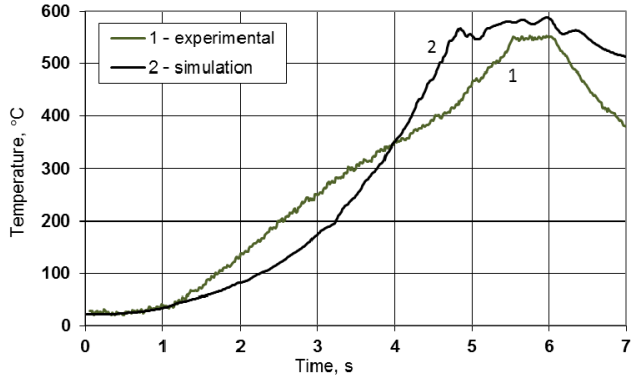

Fig. 10 Temperature on the upper side of the workpiece at the contact zone

The surface temperature variation of the simulation was obtained from the identical position where the surface temperature was measured in the experiments.

The maximum temperature value on the upper side of the workpiece at the contact zone obtained by simulation was 589ºC. The simulation and the experiments both showed very similar results.

7. Conclusions

An experimental analysis and a numerical simulation of a stainless AISI 304 steel plate were carried out.

The experiment showed that the maximum axial drilling force for a 1.5 thickness sheet of AISI304 steel is about 1480 N and the maximum torque is up to 2.5 Nm. The measured temperature on the upper side of the workpiece at the contact zone reaches 569°C.

The simulation showed that the maximum temperature in the workpiece is reached when the conical part

of the tool penetrates the workpiece. During that time, it is up to 1180 K (907ºC), and it is up to 969 K (696ºC) in the final stage of the drilling. The variation of temperature on the upper side of the workpiece at the contact zone obtained by the simulation and the experiments was very similar. The comparison of the experimental force and torque variations with the simulated ones also showed a good agreement.

The obtained results of the presented study lead to a conclusion that the presumptions taken in the simulation are correct and realistically define the friction drilling process. The computational model could be useful for prediction of rational frictional drilling regimes in order to lower drilling forces and, as a consequence, to decrease tool wear.

References

1. **Miller, S.F.; Wang, H.; Li, R.; Shih, A.J.** 2006. Experimental and numerical analysis of the friction drilling process, ASME Journal of Manufacturing Science and Engineering 128: 802-810. http://dx.doi.org/10.1115/1.2193554.
2. **Miller, S.F. Shih, A.J**. 2007. Thermo-mechanical Finite Element Modelling of the Friction Drilling Process, Journal of Manufacturing Science and Engineering 129: 531 -538. http://dx.doi.org/10.1115/1.2716719.
3. **Krasauskas, P.; Keselys, T.; Kilikevičius, S.** 2012. Experimental Investigation and Simulation of Stainless AISI 304 Steel Thermoplastic Drilling, Proceedings of 17th International Conference Mechanika: 150-154.
4. **Chow, H.M.; Lee, S.M.; Yang, L.D.** 2008. Machining characteristic study of friction drilling on AISI 304 stainless steel. Journal of Materials Processing Technology 207(1-3): 180-186. http://dx.doi.org/10.1016/j.jmatprotec.2007.12.064.
5. **Lee, S.M; Chow, H.M.; Huang, F.Y.; Yan, B.H.** 2009. Friction drilling of austenitic stainless steel by uncoated and PVD AlCrN- and TiAlN-coated tungsten carbide tools. International Journal of Machine Tools and Manufacture 49(1):81-88. http://dx.doi.org/10.1016/j.ijmachtools.2008.07.012.
6. **Johnson, G.; Cook, W.** 1983. A Constitutive Model and Data for Metals Subjected to Large Strains, High Strain Rates and High Temperatures, Proceeding of the 7th Int. Symp. On Ballistics, The Hague, the Netherlands: 1-7.
7. **Johnson, G.; Cook, W.** 1985. Fracture characteristics of three metals subjected to various strains, strain rates, temperatures and pressures. Eng. Fract. Mech. 21: 31-48. http://dx.doi.org/10.1016/0013-7944(85)90052-9.
8. Abaqus Theory Manual, version 6.2, Hibbit, Karlsson & Sorensen, Inc., 2001.
9. **Fronta´n, J. et all.** 2012. Ballistic performance of nanocrystalline and nanotwinned ultrafine crystal steel. Acta Materialia 60: 1353-1367. http://dx.doi.org/10.1016/j.actamat.2011.11.029.

P. Krasauskas, S. Kilikevičius, R. Česnavičius, D. Pačenga

NERŪDYJANČIO PLIENO AISI 304 FRIKCINIO GRĘŽIMO PROCESO EKSPERIMENTINIS TYRIMAS IR SKAITINIS MODELIAVIMAS

R e z i u m ė

Straipsnyje pateikiamas nerūdijančio plieno AISI 304 frikcinio gręžimo proceso eksperimentinė analizė ir skaitinis modeliavimas. Frikcinio gręžimo metu vyksta terminiai ir plastiniai medžiagos procesai: ruošinio ir įrankio kontakto zonoje temperatūra kinta plačiose ribose ir siekia metalo lydymosi temperatūrą, o metalas aplink formuojamą skylę smarkiai plastiškai deformuojasi. Be to, dėl įrankio formos nepastovumo, šio proceso parametrai nuolat kinta, todėl skaitinis frikcinio gręžimo modeliavimas yra sudėtingas uždavinys. Darbe buvo atliktas AISI 304 plieno frikcinio gręžimo eksperimentas, gauti ašinės jėgos ir momento eksperimentiniai duomenys buvo palyginti su baigtinių elementų metodu atlikto modeliavimo rezultatais ir padaryta išvada, kad priimtos modeliavimo prielaidos yra teisingos ir gauti rezultatai atspindi eksperimento rezultatus.

P. Krasauskas, S. Kilikevičius, R. Česnavičius, D. Pačenga

EXPERIMENTAL ANALYSIS AND NUMERICAL SIMULATION OF THE STAINLESS AISI 304 STEEL FRICTION DRILLING PROCESS

S u m m a r y

This paper deals with experimental analysis and numerical simulation of the stainless AISI 304 steel friction drilling process. During fiction drilling, thermal and plastic material processes take place: temperatures in the contact zone vary in a very wide range reaching the metal melting temperature, thus, large-sized plastic deformations occur in the material around the forming hole. Also, the parameters of this process are constantly changing during the drilling due to the complicated shape of the tool. Therefore simulation of friction drilling is a very complex problem. For this reason a friction drilling experiment was carried out. Variations of experimental axial force and torque values were obtained and compared to finite element simulation results and a conclusion was made that the presumptions taken in the simulation are correct and realistically define the friction drilling process.

Keywords: friction drilling, temperature, plastic deformation, axial force, torque, numerical simulation.

Received August 15, 2014
Accepted November 17, 2014